



AIAA 95-0337
TIME-DOMAIN AEROELASTIC
ANALYSIS OF A TWO AIRFOIL SYSTEM
WITH APPLICATION TO UNSTEADY
ROTARY WING FLOWFIELDS

K.D.Jones and M.F.Platzer
Naval Postgraduate School
Monterey, CA

33rd Aerospace Sciences
Meeting & Exhibit
January 9-12, 1995 / Reno, NV

Time-Domain Aeroelastic Analysis of a Two Airfoil System with Application to Unsteady Rotary Wing Flowfields

K. D. Jones[†] and M. F. Platzer[‡]

Naval Postgraduate School
Monterey, California

Abstract

In this paper a time-domain aeroelastic analysis code is described for single airfoils and two-foil systems in incompressible, inviscid flow. Flow solutions are obtained using a time-stepping panel code, and airfoil motions are computed using a two-degree-of-freedom (TDOF) spring/mass model. The time-stepping aeroelastic code is evaluated through comparisons with several classical frequency-domain studies for both single-degree-of-freedom (SDOF) and TDOF motions. SDOF results show excellent agreement with past studies and, furthermore, provide a look into the evolution of the motion in time. Additionally, using a two-foil system, it is shown that flutter of a trailing airfoil can be controlled by proper oscillation and phasing of a leading airfoil. TDOF results highlight a step-size dependence of the panel code, but again demonstrate the active flutter control by means of an oscillating leading airfoil. A method for simulating unsteady rotary wing flowfields with the two-foil aeroelastic code is described, and comparisons with past frequency-domain studies show good agreement.

Nomenclature

c = chord length
 C_l = lift coefficient per unit span
 C_m = pitching moment coefficient per unit span
 h = bending displacement (positive downward)
 h^* = wake spacing in rotary wing flows
 I_α = moment of inertia about the elastic axis
 k = reduced frequency, $\omega c/V_\infty$
 k_α = reduced natural pitching frequency
 k_h = reduced natural plunging frequency
 k_F = reduced flutter frequency

K_h = spring constant for plunging
 K_α = spring constant for pitching
 L = lift per unit span
 m = mass of the wing per unit span
 m^* = ω/Ω
 M = pitching moment per unit span
 $q(s)$ = source strength distribution
 r = radius of rotary wing blade section
 S_α = static moment, $x_\alpha m$
 t = time
 V_α = reduced velocity, $1/k_\alpha$
 V_∞ = freestream velocity magnitude
 x_p = leading edge to elastic axis distance
 x_α = elastic axis to center of mass distance
 X_{shift} = horizontal offset of the control airfoil
 Y_{shift} = vertical offset of the control airfoil
 α = angle of attack
 $\gamma(s)$ = Vorticity strength distribution
 Γ_K = Vorticity due to airfoil motion at K th step
 ϕ = complete velocity potential
 φ_∞ = uniform flow velocity potential
 φ_{cv} = core vortex velocity potential
 φ_s = distributed source velocity potential
 φ_v = distributed vorticity velocity potential
 φ_w = wake panel velocity potential
 λ = wake wavelength, $2\pi/k$
 ω = circular frequency
 ω_h = uncoupled natural bending freq., $\sqrt{K_h/m}$
 ω_α = uncoupled natural torsional freq., $\sqrt{K_\alpha/I_\alpha}$
 Ω = rotary wing rotational frequency
 ρ_∞ = freestream density
 τ = nondimensional time, tV_∞/c
 (\cdot) = differentiation with respect to t
 $(\cdot)'$ = differentiation with respect to τ

I. Introduction

For many decades, scientists have been aware of the danger of structural failure due to aerodynamically driven oscillations. A classic example of this phenomenon occurred in 1940 when the Tacoma Narrows bridge, driven by the ambient wind, came apart after many hours of divergent resonance.¹ This behavior,

[†] NRC Research Associate, member AIAA.

[‡] Professor, Dept. Aeronautics and Astronautics, Associate Fellow, AIAA.

This paper is declared a work of the U.S. Government and is not subject to copyright protection in the United States.

called flutter, also occurs on aircraft wings and empennages, helicopter and propeller blades and in turbomachines, such that applications for this research are plentiful. The study of these aerodynamically driven motions is referred to as aeroelasticity.

Most flutter codes used in the aerospace industry are based on linearized oscillatory aerodynamic theory as input into the flutter equations, solving the flutter problem in the frequency-domain rather than in the time-domain. However, many modern computational fluid dynamics (CFD) codes employ a time-marching approach which suggests that the use of such codes for the prediction of airfoil/blade flutter and dynamic response may become a practical approach in the near future.

The current method utilizes such a time-stepping approach with an unsteady panel method to describe the inviscid, incompressible flowfield and with a TDOF spring/mass system to model the twisting and bending of the airfoil/blade geometry. The algorithms used in the code are outlined in the following sections. Additionally, an active control loop used to suppress flutter of the trailing airfoil in a two-foil system and a method for simulating unsteady rotary wing flowfields are described. Finally, the accuracy and limitations of the approach are determined through comparisons with past theoretical and numerical studies.

II. Approach

Aeroelasticity is a multi-disciplinary subject combining aerodynamics and structural dynamics. The methods used for each of these fields are discussed in some detail in this section. The methods used to simulate the unsteady, wake-induced effects on helicopter blade flutter are outlined as well.

Aerodynamics Consider incompressible, inviscid flow over two airfoils of arbitrary geometry which may execute an arbitrary motion relative to each other. The basic governing equation for this problem is, therefore, the Laplace equation.

In the past, a number of investigators have solved the steady flow problem using source and vortex paneling, the most prominent ones being Hess and Smith.² A few authors have extended this approach to the case of unsteady motion of single airfoils, notably Basu and Hancock³ and Kim and Mook.⁴ At the Naval Postgraduate School, Teng⁵ developed a computer code for the numerical solution of unsteady, inviscid, incompressible flow over an airfoil. Teng's work was extended by Platzer et al⁶ to investigate interference effects with

multiple airfoils. Each airfoil surface is approximated by a large number of surface elements, and a uniform source distribution and vorticity distribution are placed on each element. The source strength varies from element to element, while the vortex strength is the same for all elements. The singularity strengths are determined from the flow tangency condition on both airfoil surfaces and the Kutta condition at each trailing edge. This approach currently is limited to cases where vortices shed from the upstream airfoil do not impinge directly upon the downstream airfoil. Yao and Liu,⁷ in their recent work, have been able to account for vortex impingement.

The unsteady flow problem differs from the steady flow problem in that the continuous shedding of vorticity into each foil's trailing wake needs to be included in the computation. According to the vorticity conservation theorem, any change in circulation around an airfoil must be matched by an equal and opposite vortex shed from the foil's trailing edge. The presence of the countervortices provides the flow with a kind of memory in that the flow at a particular time is affected by the bound circulation of the past. It is this nonlinearity that distinguishes the numerical technique required for the unsteady flow solution from the simpler steady flow problem of solving N linear equations in N unknowns.

The solution technique requires an iterative type solution. The present approach follows closely the original panel method of Hess and Smith, while with regard to the modeling of the wake it adopts the procedure advocated by Basu and Hancock. Uniform source and vorticity distributions are placed on each panel at time t . The wake consists of a single vorticity panel attached as an additional element on each airfoil through which the vortices are shed into the respective wake as a series of point vortices which are being convected downstream with the fluid. A uniform vorticity distribution is placed on the wake panel of each airfoil. This panel is further characterized by its length and its inclination with respect to the local frame of reference. After each time step, the vorticity of the wake panel is concentrated into a single point vortex and convected downstream. Simultaneously, a new wake panel is formed. The downstream wake of point vortices is thus formed by the shed vorticity of previous time steps.

As is well known, the overall flowfield can be built up by three simple flows, namely a uniform flow, a source flow, and a vortex flow. The velocity potentials

of these flows can be linearly superimposed, i.e.,

$$\phi = \varphi_\infty + \varphi_s + \varphi_v, \quad (1)$$

where the velocity potential of the uniform flow is given by

$$\varphi_\infty = V_\infty(x \cos \alpha + y \sin \alpha), \quad (2)$$

the velocity potential of a source distribution, $q(s)$, per unit length by

$$\varphi_s = \int \frac{q(s)}{2\pi} \ln(r) ds \quad (3)$$

and the velocity potential of a vorticity distribution, $\gamma(S)$ per unit length, by

$$\varphi_v = - \int \frac{\gamma(s)}{2\pi} \theta ds. \quad (4)$$

For the analysis of unsteady airfoil motions it is necessary to add the contributions from the previously mentioned wake panels and the trailing core vortices for each airfoil, hence

$$\phi = \varphi_\infty + \varphi_s + \varphi_v + \varphi_w + \varphi_{cv} \quad (5)$$

where the wake panels are treated as an extension of each airfoil's surface and

$$\varphi_{cv} = - \sum_{k=2}^K \frac{\Gamma_k - \Gamma_{k-1}}{2\pi} \tan^{-1} \frac{y - y_k}{x - x_k} \quad (6)$$

with K the total number of time steps and (x_k, y_k) the coordinates of the k th core vortex.

The flow tangency conditions are satisfied at the exterior mid-points (control points) of each panel. The Kutta condition postulates that the pressure on the upper and lower surface at the trailing edge of each panel be equal.

The wake panels are formed with a length and inclination to the respective local frames of reference that satisfy the Helmholtz theorem

$$\Delta_k(\gamma_w)_k + \Gamma_k = \Gamma_{k-1}. \quad (7)$$

At the next time step the wake panel is detached from the trailing edge and is convected downstream as a concentrated vortex. This unsteady flow model therefore introduces an additional boundary condition, i.e., the conservation of vorticity. However, the introduction of the wake creates three additional unknowns for

each airfoil, namely the vorticity of the wake panel, its length and its inclination. Therefore, two additional conditions are required for each airfoil in order to solve the system. The approach suggested by Basu and Hancock is extended to the two-foil case:

1. The wake panel is oriented in the direction of the local resultant velocity at the panel midpoint.
2. The length of the wake panel is proportional to the magnitude of the local resultant velocity at the panel midpoint and the size of the time step. The essential elements of this scheme are summarized in Fig. 1.

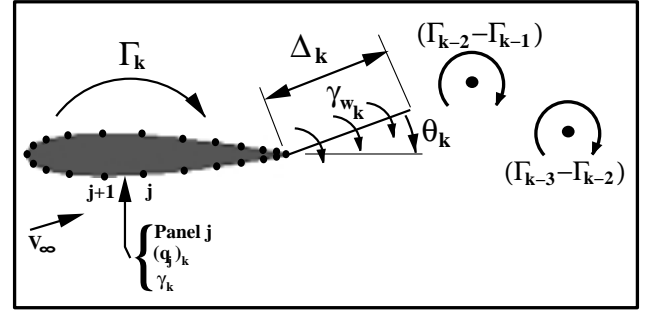


Figure 1. Schematic of the unsteady panel code.

For the development of the computational procedure, the important concept of influence coefficients is used. Formally, an influence coefficient is defined as the velocity induced at a field point by a unit strength singularity placed anywhere in the flowfield. The flow tangency and Kutta conditions require the computation of the normal and tangential velocity components at all the control points. Furthermore, as a result of the wake model additional influence coefficients need to be defined. Detailed explanations of these influence coefficients and of the solution procedure are given in Teng and in Pang.⁸ A thorough evaluation of the accuracy of the panel code was performed by Riester⁹ by comparing the computed lift and moment coefficients for both pitch and plunge motions with those of Theodorsen and Garrick.¹⁰

Structural Dynamics For the computation of motion a TDOF spring/mass system, illustrated in Fig. 2, is used to model the bending and twisting of the wing. The equations governing this motion are

$$m\ddot{h} + S_\alpha\ddot{\alpha} + m\omega_h^2 h = -L \quad (8)$$

and

$$S_\alpha\ddot{h} + I_\alpha\ddot{\alpha} + I_\alpha\omega_\alpha^2\alpha = M, \quad (9)$$

where the dots denote differentiation with respect to time. Note, Eqs. (8) and (9) assume that α is small, replacing $\cos(\alpha)$ with 1 in the coupling term, S_α .

Figure 2. Schematic of the spring/mass system.

Nondimensionalizing the system using reference values of length= c , velocity= V_∞ , time= c/V_∞ and mass= $c^2\pi\rho_\infty/4$, and rewriting the system in matrix notation, one obtains

$$[\mathbf{M}]\{X\}'' + [\mathbf{k}]\{X\} = \{F\} \quad (10)$$

where

$$[\mathbf{M}] = \begin{bmatrix} m & S_\alpha \\ S_\alpha & I_\alpha \end{bmatrix}, \quad [\mathbf{k}] = \begin{bmatrix} m\omega_h^2 & 0 \\ 0 & I_\alpha\omega_\alpha^2 \end{bmatrix},$$

$$\{X\} = \begin{Bmatrix} h \\ \alpha \end{Bmatrix} \quad \text{and} \quad \{F\} = \frac{2}{\pi} \begin{Bmatrix} -C_l \\ C_m \end{Bmatrix},$$

and where the primes denote differentiation with respect to nondimensional time.

Equation (10) is a system of two, coupled, second-order, nonlinear, differential equations, nonlinear in that C_l and C_m are functions of h and α . SDOF simulations may be performed by setting $S_\alpha = 0$ and either $m = \infty$ and $\omega_h = 0$ or $I_\alpha = \infty$ and $\omega_\alpha = 0$ for pitching-only or plunging-only motions, respectively.

Equation (10) is advanced in time by first solving for $\{X\}''$,

$$\{X\}'' = [\mathbf{M}]^{-1}\{F\} - [\mathbf{M}]^{-1}[\mathbf{k}]\{X\}, \quad (11)$$

then rewriting the result as a system of two coupled, 1st-order equations

$$\begin{aligned} \{X\}' &= \{Y\} \\ \{Y\}' &= [\mathbf{M}]^{-1}\{F\} - [\mathbf{M}]^{-1}[\mathbf{k}]\{X\}, \end{aligned} \quad (12)$$

and, finally, integration is performed using either a 2nd-order modified Euler scheme or a 4th-order Runge-Kutta scheme. Note that the iterative modified Euler scheme reduces to a 2nd-order Runge-Kutta scheme if just two iterations are used.

The TDOF spring/mass integration procedure was validated by setting $C_l = C_m = 0$ (simulating an undamped system) and computing the total energy (kinetic and potential) of the system at each time step. With just 30 steps per cycle the 4th-order scheme computed about a 0.005% loss in total energy per cycle for coupled or uncoupled motions.

Rotary Wing Flowfields Simulations of wake interference in rotary wing flowfields are performed in a two-dimensional, strip-theory fashion similar to the approach of Loewy.¹¹ Loewy approximated the helical wake structure beneath a hovering helicopter at a given radial station as a two dimensional flow with a single blade section with an infinite series of wakes beneath it, as shown in Fig. 3a. The wake separation, h^* , was a function of the inflow velocity, and the phasing was determined by the ratio of the pitching frequency to the rotational frequency, $m^* = \omega/\Omega$. To simplify computations, Loewy assumed that these wakes extended to $\pm\infty$.

Figure 3. Schematics for rotary wing simulations.

In the present approach only a single, finite-length wake is considered, and this is facilitated by placing a second blade upstream a distance $2\pi r$ (the circumferential length for the radial station, r), and below the first blade the distance h^* , as portrayed in Fig. 3b. The reduced pitching frequency is determined directly from the specified frequency ratio, $k = m^*/r$.

III. Results

The following subsections present results of single- and two-airfoil systems with SDOF and TDOF motions. Additionally, an active control loop for two-airfoil systems is introduced, and sample results are given, followed by simulations of wake interference in rotary wing flowfields.

Single Airfoil SDOF Results for a single airfoil undergoing pitching motions are compared with the classical works of Theodorsen and Garrick and of Smilg¹² and the more contemporary work of Turner.¹³ Theodorsen and Garrick considered the pitching motion of a flat plate with arbitrary k_α and I_α about a specified elastic axis, x_p . They showed that k_F was independent of I_α , and for $x_p = 0$, $k_F \approx 0.08$.

The present method introduces a perturbation angle of attack displacement at $\tau = 0$, and computes the resulting motion as a function of time. Sample time histories of α are given in Fig. 4 at a stable, a neutral and an unstable frequency for a NACA 0007 airfoil with $I_\alpha = 150$.

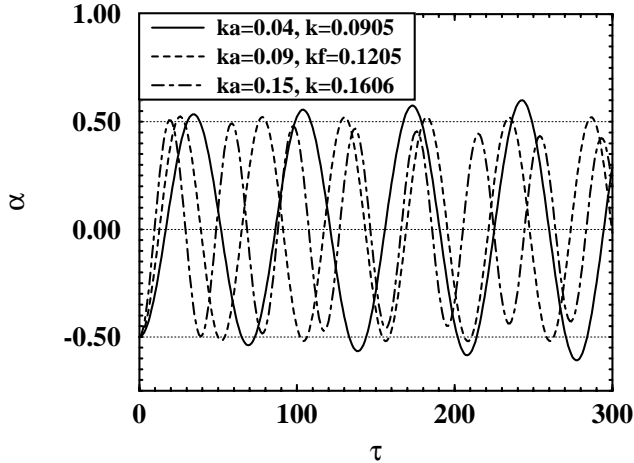


Figure 4. SDOF time history of α .

The frequency response predicted by the present approach is compared to the flat-plate results in Fig. 5 for a spectrum of airfoil thicknesses and I_α 's. Each cluster of 3 curves corresponds to the value of I_α indicated in the legend, with the lower, middle and upper line of each group corresponding to a NACA 0001, NACA 0007 and NACA 0012 airfoil, respectively. The \circ , \square and \diamond symbols are located at the predicted flutter frequencies, k_F , for the different airfoils and I_α values (i.e., the frequency where a constant amplitude oscillation is maintained). Note that for each of the NACA airfoils k_F is constant with respect to I_α , and even

though the frequency response does not change much with thickness, the flutter frequency changes significantly. As I_α increases, the effect of thickness becomes less apparent in the curves, and the curves rapidly approach the theoretical undamped response for $I_\alpha = \infty$.

According to Smilg, a flat plate will not flutter for I_α less than about 143. This is indicated by the frequency response curves shown in Fig. 5. For I_α lower than about 150 the response curves do not intersect the line $k_F = 0.08$.

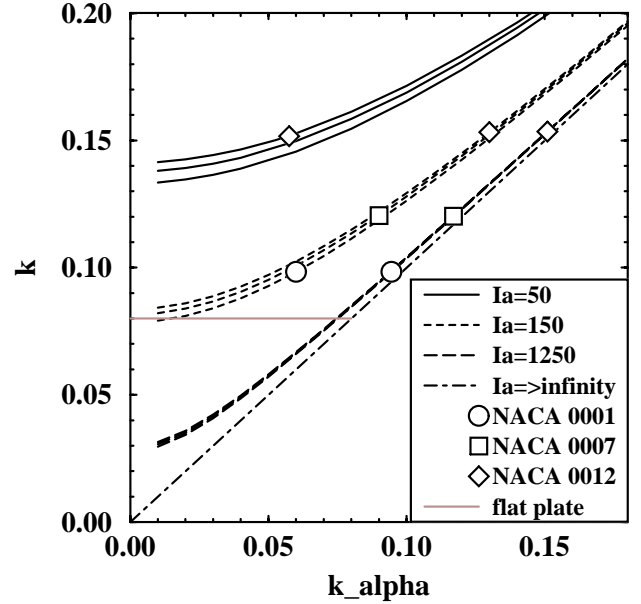


Figure 5. SDOF frequency response for $x_p = 0$.

The relationship for k_α/k_F as a function of I_α is derived from flat plate theory as $k_\alpha/k_F = \sqrt{1 + 143/I_\alpha}$. This curve is plotted with those predicted by the present scheme in Fig. 6 for several airfoil thicknesses. It can be seen that as the airfoil thickness approaches zero the time-domain results approach flat-plate theory.

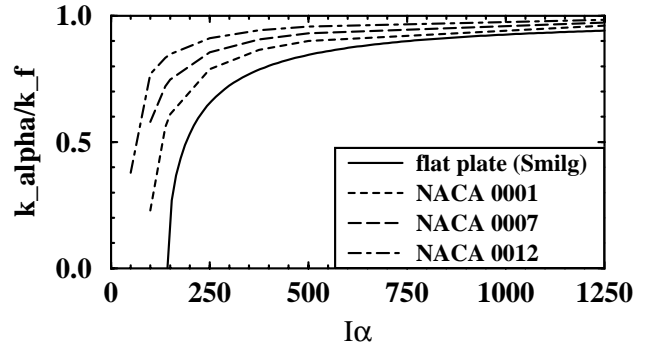


Figure 6. Frequency ratio dependence on I_α .

The method employed by Turner used the current panel code, pitching the airfoil sinusoidally. Sinusoids were fit to the resulting C_m curve, and stability was determined by the sign of the out-of-phase portion. For a NACA 0007 airfoil Turner predicted $k_F \approx 0.115$, whereas the present method predicts $k_F \approx 0.120$. Both methods found a slight step-size dependence in the predicted amplitudes of C_l and C_m but found this to be inconsequential in the resulting SDOF motion and flutter frequencies.

Single Airfoil TDOF Data for a single airfoil with both pitching and plunging motions are available for comparison from Theodorsen and Garrick and Turner. Unfortunately, while the small step-size dependence of C_l and C_m did not affect the SDOF motion appreciably, they do affect the TDOF motion. In Fig. 7 the stability bounds predicted by flat-plate theory and Turner are shown with the stability bounds predicted by the new code for several step-sizes and with $m = 2$, $I_\alpha = 0.125$, $x_p = 0.3$ and $x_\alpha = 0.1$. Turner's results predicted less stable behavior than flat-plate theory, arguably due to the finite airfoil thickness (NACA 0007) used by Turner.

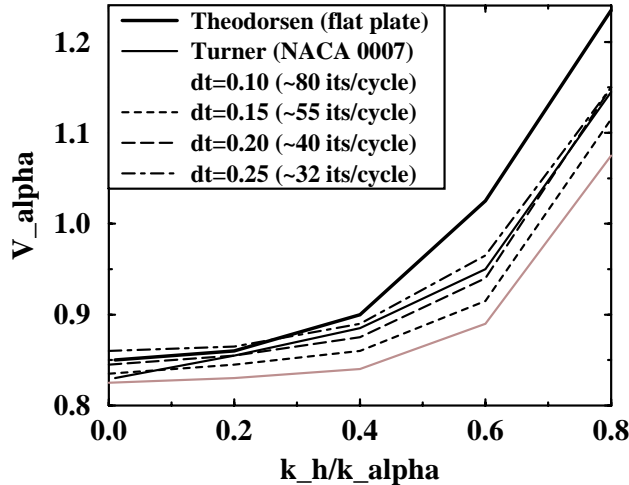


Figure 7. TDOF flutter boundaries.

Turner's results were not greatly affected by the amplitude errors, since only the phase relationships between the motion and C_l and C_m were used to predict stability. On the other hand, since the airfoil motion computed by the new code is directly determined by the amplitudes of C_l and C_m , any errors feed back into the solution, such that the error grows in time. Qualitatively, the shape of the stability bound is con-

sistent with Turner, but no quantitative statement can be made.

Two Airfoil SDOF Airfoil/wake interference simulations with two airfoils are compared to the frequency-domain work of Turner. For these cases the leading or control airfoil is pitched sinusoidally between $\alpha = \pm 0.5^\circ$ with $k = 0.1$, $Y_{shift} = -2.0$, $x_p = 0$ and with chord lengths of 1, $1/2$, $1/4$ and $1/10$. The trailing airfoil starts at $\alpha = -0.5^\circ$ and is released in sync with the control airfoil with $x_p = 0$, $I_\alpha = 150$ and $k_\alpha = 0.0585$. In the absence of the leading airfoil these conditions yield an unbounded pitching motion with $k = 0.1$. The value of X_{shift} is varied between 0 and -63. In nondimensional space the wake wavelength is $\lambda = 2\pi/k$ or roughly 63.

Values of X_{shift} resulting in flutter suppression or amplification agree well with Turner. Sample plots are shown in Fig. 8 for cases that are initially stable, neutral and unstable.

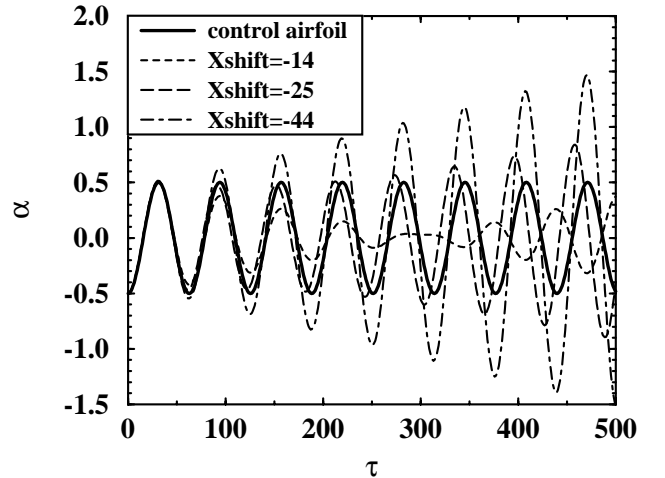


Figure 8. Two airfoil wake interference with pitching.

Flutter is suppressed at $X_{shift} = -14$ ($\approx -\lambda/4$), and flutter is amplified at $X_{shift} = -44$ ($\approx -3\lambda/4$). Note, while the control airfoil used in Fig. 8 has a chord length of 1, results with smaller control airfoils are similar, with slightly lower damping rates.

Of particular interest here is the evolution of the free airfoil's motion in time; a facet of the problem not captured by the frequency-domain methods. The motion with $X_{shift} = -14$, although initially stable, changes phase by 180° and becomes unstable once the pitch magnitude becomes small. This phase/magnitude relationship is illustrated in Fig. 9. The phase of the case that is initially unstable remains unchanged for all time, but the phase for the case that

is initially neutral begins to drift toward an unstable mode immediately. This tendency for the phase to drift to unstable modes was previously observed by Bahkle et al.¹⁴

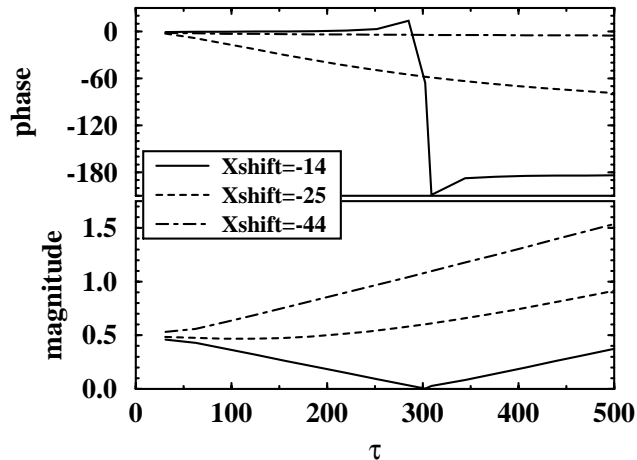


Figure 9. Trailing airfoil Phase/magnitude relation.

The stabilizing/destabilizing effect of wake interference is perhaps most easily understood by observing the phase relationship between the impinging wake's vorticity (positive counterclockwise) and the angular acceleration of the free airfoil (positive clockwise), shown in Fig. 10.

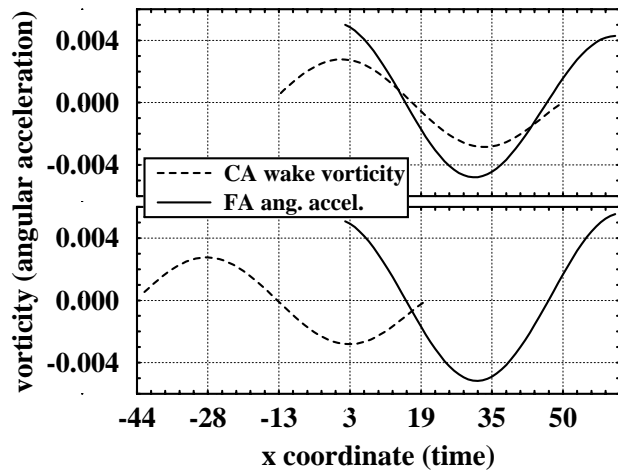


Figure 10. Vorticity/acceleration phase relationship.

With $X_{shift} = -14$ (upper graph) flutter is suppressed, and it can be seen that the vorticity and acceleration are in-phase (Note, due to the above definitions, in-phase means that they have an opposite sense of rotation). For $X_{shift} = -44$ (lower graph) the vorticity

and acceleration are out-of-phase and the motion is unbounded.

Two Airfoil TDOF Due to the time-step dependency discovered in the single airfoil TDOF simulations a quantitative study of two airfoil TDOF motion is not possible with the current approach. However, a qualitative analysis is still useful, primarily in demonstrating the flutter suppression capabilities of an upstream control airfoil.

In the included simulations the free airfoil has $x_p = 0.3$, $x_\alpha = 0.1$, $m = 2$, $I_\alpha = 0.125$, $k_\alpha = 1.18$ and $k_h = 0$. In the absence of the control airfoil these settings result in rapidly divergent motion with $k = 0.73$ ($V_\alpha = 1.37$). The control airfoil is located at $Y_{shift} = -2$ and X_{shift} values of $\approx -\lambda/4$ and $\approx -3\lambda/4$, where $\lambda \approx 8.59$. Time history plots of α are shown in Fig. 11 for the two cases.

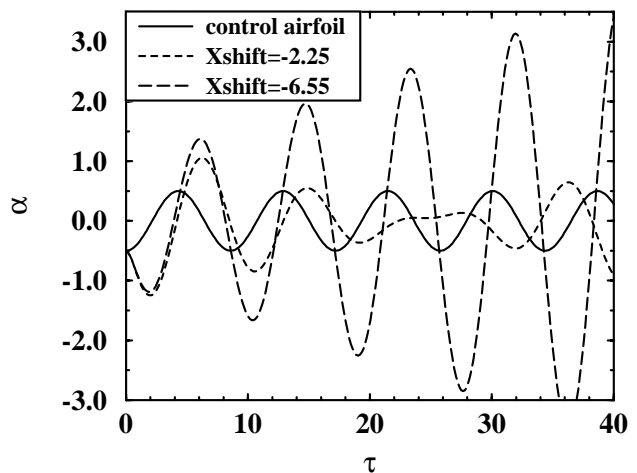


Figure 11. TDOF wake interference.

As with the SDOF case, for $X_{shift} \approx -\lambda/4$ flutter is initially suppressed and with $X_{shift} \approx -3\lambda/4$ it is promoted. Unfortunately, as with the SDOF case, flutter suppression is only temporary, as the motion of the free airfoil drifts from a stable to an unstable phase angle, and the pitching diverges.

Active Control Loop The short-lived success of flutter suppression in the above cases suggests the use of an active control loop for determining appropriate motions of the control airfoil to maintain stability. The simplest approach is to place the control airfoil at $-\lambda/4$ and pitch it exactly as the free airfoil pitches, thereby correcting for any phase changes of the free airfoil. This approach works; unfortunately, the rate at which the pitch oscillations are damped is proportional to the impinging wake's vorticity magnitude which, in

turn, is proportional to the pitching magnitude of the control airfoil. Consequently, pitching of the free airfoil is suppressed, but at a rate like $1/\tau$, such that the motion is not completely damped until $\tau = \infty$.

A somewhat more robust feedback loop pitches the control airfoil with an approximately constant magnitude and with the same phase as the free airfoil. When the free airfoil motion is damped to a small amplitude, the new approach reverts to the first method suggested. This control loop is quite successful, as shown in Fig. 12.

Airfoil separations other than $-\lambda/4$ are possible if an appropriate signal phase delay is given; however, due to the increased time delay required for the control airfoil's wake vorticity to convect downstream to the free airfoil, complete damping becomes difficult.

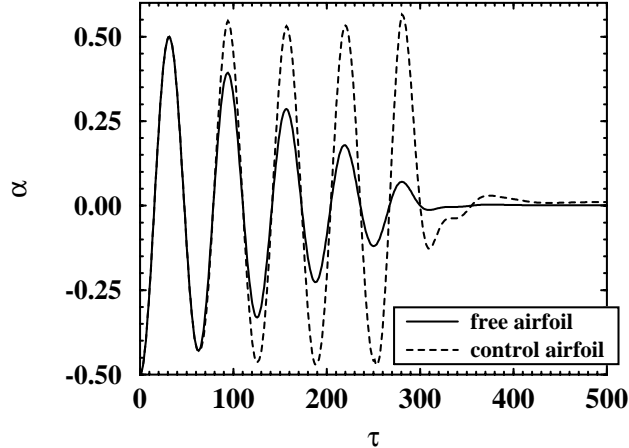


Figure 12. Flutter suppression using active control.

All spring/mass settings for the reference foil are the same here as the case presented in Fig. 8. The control airfoil is located at $X_{shift} = -14$ and $Y_{shift} = -2$ and has a chord length of $1/2$.

Rotary Wing Flows As indicated in Fig. 3, wake interference for a single-bladed rotary wing flow (e.g., Loewy's equivalent single bladed rotor) is simulated here by pitching an upstream blade whose wake represents the reference blade's wake after one rotation of the rotor system. To further enhance the accuracy of this wake model the first feedback loop option is used such that pitching motions of the reference blade are exactly matched by the upstream blade, thereby generating an identical wake.

In Fig. 13 the effect of wake interference from the preceding blade on the pitch stability of the reference blade is shown for pitch oscillations about the leading edge, $x_p = 0$. The blade has a NACA 0007

profile, $I_\alpha = 375$ and $Y_{shift} = -h^* = -2.5$. The present time-domain approach provides the decay or growth of the pitch oscillation; therefore, the time rate of change of pitching amplitude is a convenient measure of the stability or instability of the pitch oscillation which is plotted on the ordinate of Fig. 13 as a function of Loewy's frequency ratio, $m^* = \omega/\Omega$, on the abscissa. For conventional cyclic inputs $m^* = 1$, since blade pitching is mechanically coupled to blade rotation via the swashplate, but for higher harmonic control (HHC) and multi-bladed rotor systems m^* will typically be non-integer. Since $k = m^*/r$, a variation of m^* implies a variation of k for a given radial station r which, in turn, means a relative shifting of the phase between the impinging wake's vorticity and the reference blade's angular acceleration, as previously discussed with reference to Fig. 10. In Fig. 13, $r = 8$ resulting in $X_{shift} \approx 50$.

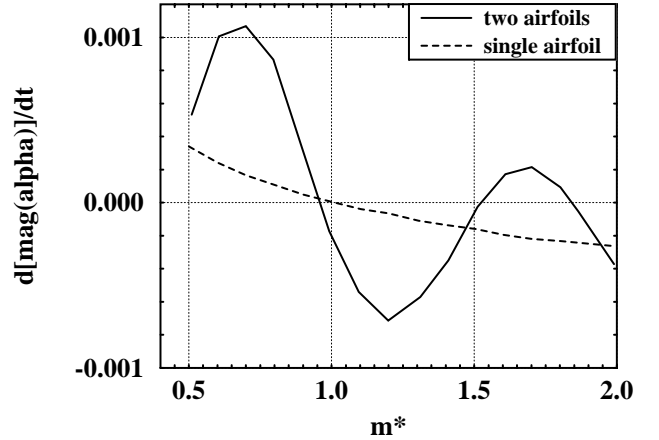


Figure 13. Rotary wing stability.

As pointed out in the SDOF section, a single airfoil becomes unstable at reduced frequencies below about 0.12. This corresponds to $m^* = kr = 0.96$, as shown by the dashed line in Fig. 13. While the single blade was stable for $k > 0.12$ ($m^* > 0.96$), the inclusion of wake interference from the preceding blade produces a second region of instability for $1.52 \leq m^* \leq 1.84$ ($0.19 \leq l \leq 0.23$). The stabilizing/destabilizing effect of the impinging wake is essentially sinusoidal with period m^* , enhancing stability through half the cycle and instability for the other half. The magnitude of this stability enhancement diminishes with increasing m^* , such that for higher values of m^* no instability occurs. Loewy, in Fig. 15 of reference 10, shows a similar phenomenon.

Conclusions

A time-stepping flutter analysis code was introduced, combining an unsteady, two-foil panel code with a TDOF spring/mass motion algorithm for inviscid, incompressible simulations. The utility and limitations of the approach were demonstrated through comparisons with past frequency-domain studies.

Computed SDOF pitching results agreed well with the frequency-domain results and provided the additional capability to analyze the evolution of the motion in time. Qualitatively, trends in frequency response due to sectional thickness and moment of inertia were clearly correct, and quantitative agreement was within the expected bounds afforded by the panel method.

Computed TDOF results highlighted a step-size sensitivity of the unsteady panel code which prevented a quantitative determination of TDOF flutter boundaries. Future work will replace the panel code with an Euler/Navier-Stokes solver hopefully alleviating this deficiency.

An active control loop algorithm was developed, and the included results demonstrated its success in suppressing flutter. These simulations indicated that the controlling airfoil remained effective even with greatly reduced chord lengths, but that effectiveness was lost as the distance between the foils increased. This suggests that a closely placed canard or leading edge flap may be sufficient for controlling flutter.

Wake interference in rotary wing flowfields was modelled by placing a second airfoil an appropriate distance to simulate the blade's wake from the previous revolution. The computed stability boundaries agreed well with past frequency domain studies.

The time-domain approach presented here is quite robust and efficient. Typical single airfoil simulations run on a workstation in about thirty minutes. The active control loop and rotary wing simulations demonstrate just a few of the many applications of the time-domain approach.

Acknowledgments

The first author gratefully acknowledges the support received from the Naval Postgraduate School through the National Research Council Associateship program.

References

¹ Sisto, F., "Introduction and Overview," AGARDograph No. 298, **AGARD Manual on Aeroelasticity in Axial-Flow Turbomachines: Volume 1,**

Unsteady Turbomachinery Aerodynamics, Eds. Platzer, M. F. and Carta, F. O., 1987.

² Hess, J. L. and Smith, A. M. O., "Calculation of Potential Flow about Arbitrary Bodies," **Progress in Aeronautical Sciences**, Vol. 8, pp. 1-138, Pergamon Press, Oxford, 1966.

³ Basu, B. C. and Hancock, G. J., "The Unsteady Motion of a Two-Dimensional Aerofoil in Incompressible Inviscid Flow," **Journal of Fluid Mechanics**, Vol. 87, 1978, pp. 159-168.

⁴ Kim, M. J. and Mook, D. T., "Application of Continuous Vorticity Panels to General Unsteady Incompressible Two-Dimensional Lifting Flows," **Journal of Aircraft**, Vol. 23, No. 6, 1986, pp. 464-471.

⁵ Teng, N. H., "The Development of a Computer Code for the Numerical Solution of Unsteady, Inviscid and Incompressible Flow over an Airfoil," Master's Thesis, Naval Postgraduate School, Monterey, CA, June 1987.

⁶ Platzer, M. F., Neace, K. S. and Pang, C. K., "Aerodynamic Analysis of Flapping Wing Propulsion," AIAA Paper No. 93-0484, Jan. 1993.

⁷ Yao, Z. X. and Liu, D. D., "Vortex Dynamics of Blade-Blade Interaction," AIAA Paper No. 94-0737, Jan. 1994.

⁸ Pang, C. K., "A Computer Code for Unsteady Incompressible Flow past Two Airfoils," Aeronautical Engineer's Thesis, Naval Postgraduate School, Monterey, CA, Sept. 1988.

⁹ Riester, P. J., "A Computational and Experimental Investigation of Incompressible Oscillatory Airfoil Flow and Flutter Problems," Master's Thesis, Naval Postgraduate School, Monterey, CA, June 1993.

¹⁰ Theodorsen, T. and Garrick, I. E., "Mechanism of Flutter," NACA TR-685, 1940.

¹¹ Loewy, R. G., "A Two-Dimensional Approximation to the Unsteady Aerodynamics of Rotary Wings," **Journal of the Aeronautical Sciences**, Vol. 24, No. 2, Feb. 1957, pp. 81-106.

¹² Smilg, B., "The Instability of Pitching Oscillations of an Airfoil in Subsonic Incompressible Potential Flow," **Journal of the Aeronautical Sciences**, Vol. 16, No. 11, Nov. 1949, pp. 691-696.

¹³ Turner, M., "A Computational Investigation of Wake-Induced Airfoil Flutter in Incompressible Flow and Active Flutter Control," Master's Thesis, Naval Postgraduate School, Monterey, CA, March, 1994.

¹⁴ Bakhle, M. A., Reddy, T. S. R., and Keith, T. G. Jr., "Time Domain Flutter Analysis of Cascades Using a Full-Potential Solver," **AIAA Journal** Vol. 30, No. 1, Jan. 1992, pp. 163-170.